Kwon et al. *NPG Asia Materials* (2018) 10: 659-669
DOI 10.1038/s41427-018-0060-3

NPG Asia Materials

ARTICLE Open Access

A rational method to kinetically control the rate-determining step to explore efficient electrocatalysts for the oxygen evolution reaction

Nam Hee Kwon[1], Minho Kim[2], Xiaoyan Jin[1], Joohyun Lim[1], In Young Kim[1], Nam-Suk Lee[3], Hyungjun Kim[2] and Seong-Ju Hwang[1]

Abstract

A novel, rational, and efficient way to explore high-performance electrocatalysts was developed by controlling the reaction kinetics of the rate-determining step (RDS). Density functional theory (DFT) calculations demonstrate that the RDS for the oxygen evolution reaction driven by transition metal hydroxides/oxides, i.e., surface adsorption of OH^-/OOH^* species, can be significantly promoted by increasing the electrophilicity of electrocatalysts via hybridization with electron-withdrawing inorganic nanosheets. As predicted by DFT calculation, the hybridization of Ni–Fe-layered double hydroxide (LDH)/Ni–Co-LDH, with RuO_2 nanosheets (1.0 wt%) leads to significant lowering of the overpotentials to 207/276 mV at 10 mA cm^{-2}, i.e., one of the smallest overpotentials for LDH-based materials, with the increase in the current density. The necessity of a very small amount of RuO_2 nanosheets (1.0 wt%) to optimize the electrocatalyst activity highlights the remarkably high efficiency of the RuO_2 addition. The present study underscores the importance of kinetic control of the RDS via hybridization with electron-withdrawing species for exploring novel efficient electrocatalysts.

Introduction

Electrocatalyst materials for the oxygen evolution reaction (OER), hydrogen evolution reaction (HER), oxygen reduction reaction (ORR), and CO_2 reduction reaction have attracted enormous research interest because of their crucial roles in many energy-related technologies, such as metal-air batteries, water electrolysis, fuel cells, and artificial photosynthesis[1,2]. These redox reactions require the simultaneous transfer of four or two electrons, which makes them very sluggish. Although there are several noble metals and their alloys showing excellent electrocatalyst activities[3–5], the high cost and limited abundance of noble metal elements frustrate their practical use. To replace these precious materials, a great deal of research effort has been devoted to exploring transition metal oxide/hydroxide-based electrocatalysts with low cost and high abundance[6,7]. Layered transition metal hydroxides like Ni–Co-layered double hydroxide (LDH) and Ni–Fe-LDH have received prime attention because of their excellent electrocatalytic activities for diverse electrochemical reactions, including the OER[8]. The absence of noble metal components renders these materials promising alternatives to commercial Ir/C as OER electrocatalysts. The great flexibility in the chemical compositions of these materials provides useful opportunities to enhance their electrocatalytic

Correspondence: Hyungjun Kim (linus16@kaist.ac.kr) or Seong-Ju Hwang (hwangsju@ewha.ac.kr)
[1]Center for Hybrid Interfacial Chemical Structure (CICS), Department of Chemistry and Nanoscience, College of Natural Sciences, Ewha Womans University, Seoul 03760, Republic of Korea
[2]Department of Chemistry and Graduate School of EEWS, Korea Advanced Institute of Science and Technology (KAIST), Daejeon 34141, Republic of Korea
Full list of author information is available at the end of the article.
These authors contributed equally: Nam Hee Kwon, Minho Kim

functionalities[9,10]. However, the electrocatalytic performances of these transition metal hydroxides are still inferior to those of noble metal catalyst, which prompts research efforts to improve their electrocatalytic activities. Since the functionality of electrocatalysts is generally strongly dependent on the surface area, number of active sites, and electrical conductivity, many attempts have been made to optimize these characteristics[11,12]. In one instance, hybridization with highly conductive carbon nanostructures was quite effective in enhancing the electrocatalytic activity of transition metal hydroxide/oxide materials by increasing the electrical conductivity[13]. Also, the formation of low-dimensional nanostructures with expanded surface areas, such as exfoliated two-dimensional (2D) nanosheets (NSs), is quite effective in enhancing the electrocatalytic functionality[14]. Despite these previous attempts, a novel synthetic strategy based on the electrocatalyst reaction mechanism is still necessary to explore highly efficient electrocatalysts using economically feasible transition metal oxides/hydroxides. According to previous mechanism studies on the OER process catalyzed by oxides and oxyhydroxides, the attachment of reaction intermediate OH^- and/or $OOH^•$ species on surface active sites has a profound effect on the reaction kinetics as the rate-determining step (RDS)[15,16]. Thus, it is crucial to tailor the binding affinities of sites on the surface of metal hydroxides for these intermediate species to improve the OER functionality. Since hydrophilic RuO_2 NSs can act as an efficient electron reservoir for many inorganic solids[17,18], hybridization with this electron-withdrawing NS is expected to be quite effective in enhancing the electrophilicity of transition metal hydroxides/oxides via interfacial electron transfer between hybridized NSs. The resulting increase in the electrophilicity of the electrocatalyst would be quite advantageous in promoting the binding of nucleophilic OH^- and/or $OOH^•$ species on the surface, leading to remarkable enhancement of the OER electrocatalytic activity. Thus, hybridization with this electron-withdrawing, inorganic NS can provide a novel, effective way to enhance the OER electrocatalytic activity of transition metal hydroxides/oxides. Although there are several previous reports about the synthesis of LDH-based hybrid-type electrocatalysts for OERs[10–14], no attempt has been made to improve the reaction kinetics of the OER process via fine-tuning the electrophilicity of the LDH. At the time of this submission, we are unaware of any other report about the enhancement of the electrocatalyst functionality and RDS kinetics using transition metal hydroxides/oxides via hybridization with inorganic NSs based on detailed speculation of the reaction mechanism.

Here we report an efficient method to explore economically feasible transition metal hydroxide/oxide-based OER electrocatalysts with unusually low overpotential via kinetic control of the RDS of the electrocatalytic reaction. The effects of hybridization with RuO_2 NSs on the mechanism of the OER process were quantitatively investigated with theoretical density functional theory (DFT) calculations. Based on these results, novel OER electrocatalysts, e.g., LDH–RuO_2 nanohybrids, were synthesized by hybridization of exfoliated LDH NSs with a small amount of RuO_2 NSs (≤1.5 wt%). The crystal structure, pore structure, and chemical bonding character of the resulting LDH–RuO_2 nanohybrids were systematically investigated to understand the effect of RuO_2 hybridization on these properties. The OER activity of the obtained LDH–RuO_2 nanohybrid with a very small Ru content (~0.7 wt%) is one of the best among the reported values of LDH-based electrocatalysts, underscoring the remarkably high efficiency of hybridization with RuO_2 NSs.

Experimental procedures

Theoretical simulations

The DFT calculations were performed using Vienna ab initio Simulation Package (VASP) 5.4.1[19,20] and project augmented wave function method[21,22]. The spin-polarized Perdew-Burke-Ernzerhof functional[23] was chosen for the DFT calculation. For a better description of Ni–Co-LDH, a Hubbard-U correction (DFT + U) method[24] was included using $U = 3.0$ for Ni and $U = 3.5$ for Co[25]. The vacuum was set to be 15 Å thick. The geometry optimization was completed until the total energy change between the two last ionic steps was $<1 \times 10^{-5}$ eV Å^{-1}. The optimized structures are illustrated in Figure S1 of the Supplementary Information, and the convergence processes are depicted in Figure S2 of Supplementary Information. The kinetic energy cutoff was 500 eV, and a $7 \times 6 \times 1$ Monkhorst-Pack grid was used. We used Gaussian smearing with a width of 0.2 eV for stable convergence of the self-consistent field calculation. The Bader charge analysis was performed by using the method of Henkelman et al.[26–28]. The three-dimensional charge difference map was plotted by using VESTA v3.4.0[29], and the planar averaged charge difference was obtained by using VASPkit 0.3[30]. To estimate the Gibbs free energy change of the reduction steps, we calculated the zero-point correction energy and entropic contribution at 298.15 K ($\Delta G = \Delta E + \Delta ZPE - T\Delta S$ at standard condition). The reference potential was set as the half reaction for the reversible hydrogen electrode (RHE) under alkaline conditions ($2H_2O(l) + 2e^- \rightarrow H_2(g) + 2OH^-(aq)$) by relating the chemical potential of the OH^- species as $\mu(OH^-) = \mu(H_2O) - \frac{1}{2}\mu(H_2) + \mu(e^-) + eU$, where U is the external bias voltage. The solvation energy of water was adopted from the experimental heat of vaporization[31]. The reference energy for the gaseous O_2 was corrected to yield the calculated total energy sum of

the OER pathway as 1.229 eV per electron[32] because of the well-known difficulties in obtaining an accurate energy of open-shell triplet O_2 within DFT[33].

Sample preparation

The precursors of the RuO_2 NSs, Ni–Co-LDH, and Ni–Fe-LDH NSs were prepared by exfoliation processes of the corresponding layered solids[34–36]. The exfoliation of Ni–Co-LDH/Ni–Fe-LDH was achieved with a dispersion of the pristine LDH materials in formamide, whereas the exfoliated RuO_2 NSs were obtained by intercalation of tetrabutylammonium ions into protonated $Na_{0.2}RuO_2$[35]. The exfoliated LDH NSs possessed a positive layer charge, whereas the exfoliated RuO_2 NSs were negatively charged (see Figure S3 in the Supplementary Information). The opposite surface charges of these NSs made their electrostatically driven self-assembly possible. As illustrated in Fig. 1, Ni–Co-LDH–RuO_2 nanohybrids with variable RuO_2 contents were synthesized by restacking two kinds of colloidal suspensions of oppositely charged LDHs and RuO_2 NSs for 1 day at room temperature. The resulting nanohybrids with RuO_2 contents of 0.5, 1.0, and 1.5 wt% were denoted as **NCR05**, **NCR10**, and **NCR15**, respectively. A variable amount of 0.1 M Na_2CO_3 solution was also added to maintain the charge neutrality. The obtained precipitates were washed with ethanol and distilled water and dried at 50 °C under vacuum. Additionally, the exfoliated Ni–Fe-LDH NSs were also hybridized with RuO_2 NSs. The resulting Ni–Fe-LDH–RuO_2 nanohybrid with a RuO_2 content of 1.0 wt% was denoted as **NFR10**.

Characterization

The zeta potentials of the colloidal suspensions of NSs were measured using a Malvern Zetasizer Nano ZS (Malvern, UK) instrument. The crystal structures of the present materials were examined by powder X-ray diffraction (XRD) analysis (Rigaku D/Max-2000/PC, Ni-filtered Cu Kα radiation, 25 °C). The crystal morphologies of the obtained materials were probed with field emission-scanning electron microscopy (FE-SEM) using a JEOL JSM-6700F microscope. High-resolution transmission electron microscopy (HR-TEM) images of the present materials were obtained with a JEOL JEM-2100F microscope at an accelerating voltage of 200 kV. Energy dispersive spectrometry (EDS)-line scanning and energy-filtered transmission electron microscopy (EFTEM)-elemental mapping analyses were carried out to probe the spatial elemental distributions of the hybrid materials. The chemical bonding state of the RuO_2 NSs in the present nanohybrids was investigated by Fourier transformed-infrared spectroscopy using a JASCO FT/IR-6100 FT spectrometer. The local structures of the nanohybrids were studied using X-ray absorption spectroscopy (XAS). All the XAS data were collected at beam line 10C of the Pohang Accelerator Laboratory (Pohang, Korea) in transmission mode. The surface areas of the present materials were monitored using N_2 adsorption-desorption isotherm measurements at 77 K (Micromeritics ASAP 2020). The interfacial charge transfer between the LDHs and RuO_2 NSs was examined with X-ray photoelectron spectroscopy (XPS, Thermo VG, UK).

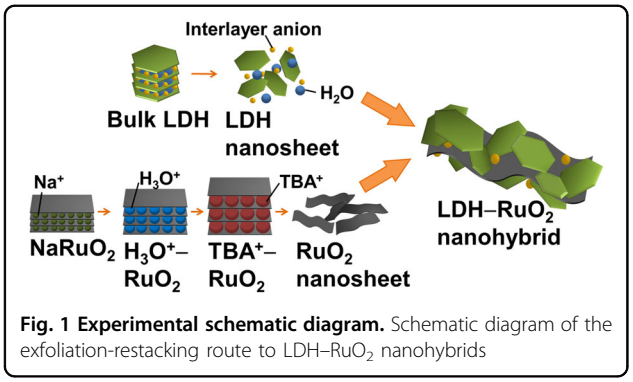

Fig. 1 Experimental schematic diagram. Schematic diagram of the exfoliation-restacking route to LDH–RuO_2 nanohybrids

Measurement of the electrocatalytic activity

The electrochemical measurements were performed at room temperature using an IVIUM analyzer with a typical three-electrode cell. A rotating ring-disk electrode-3A (ALS) was used as a rotator. The catalyst ink was prepared by dispersing 7 mg of active material, 3 mg of carbon black (Vulcan-XC72R), and 25 µl of a 5 wt% Nafion solution (Sigma-Aldrich) in an isopropanol/water (1/4, vol/vol) mixed solvent by sonication for 1 h. A total of 10 µl of catalyst ink was dropped onto a glassy carbon (GC) electrode (3 mm, ALS), which was oven-dried at 50 °C. A Pt wire and saturated calomel electrode were used as the counter electrode and reference electrode, respectively. All measurements were carried out in an O_2-saturated 1 M KOH solution. The potentials were referenced to the RHE according to the Nernst equation, $E(\mathrm{RHE}) = E(\mathrm{SHE}) + 0.241_2 + 0.059 \times \mathrm{pH}$ (at 25 °C). The electrocatalytic OER performance was examined by linear sweep voltammetry (LSV), which was measured with a rotating speed of 1600 rpm at a scan rate of 5 mV s^{-1} from 1.15 to 1.75 V (vs. RHE) for **NCR** and from 1.15 to 1.65 V (vs. RHE) for **NFR**. The current density (j) was calculated from the ratio of the current over the surface area of the GC (0.071 cm^2). The dependence of the charging current density on the scan rate was measured by cyclic voltammetry (CV) in the potential range from 0.9964 to 1.0964 V (vs. RHE) to cover the open circuit potential of 1.0744 V (vs. RHE). Electrochemical impedance spectroscopy (EIS) data were collected at 1.6 V (vs. RHE) for **NCR** and 1.5 V (vs. RHE) for **NFR** with a frequency range of 0.1–10 000 Hz. Chronopotentiometry was performed at 10 mA cm^{-2} using rotating electrodes with O_2 bubbling.

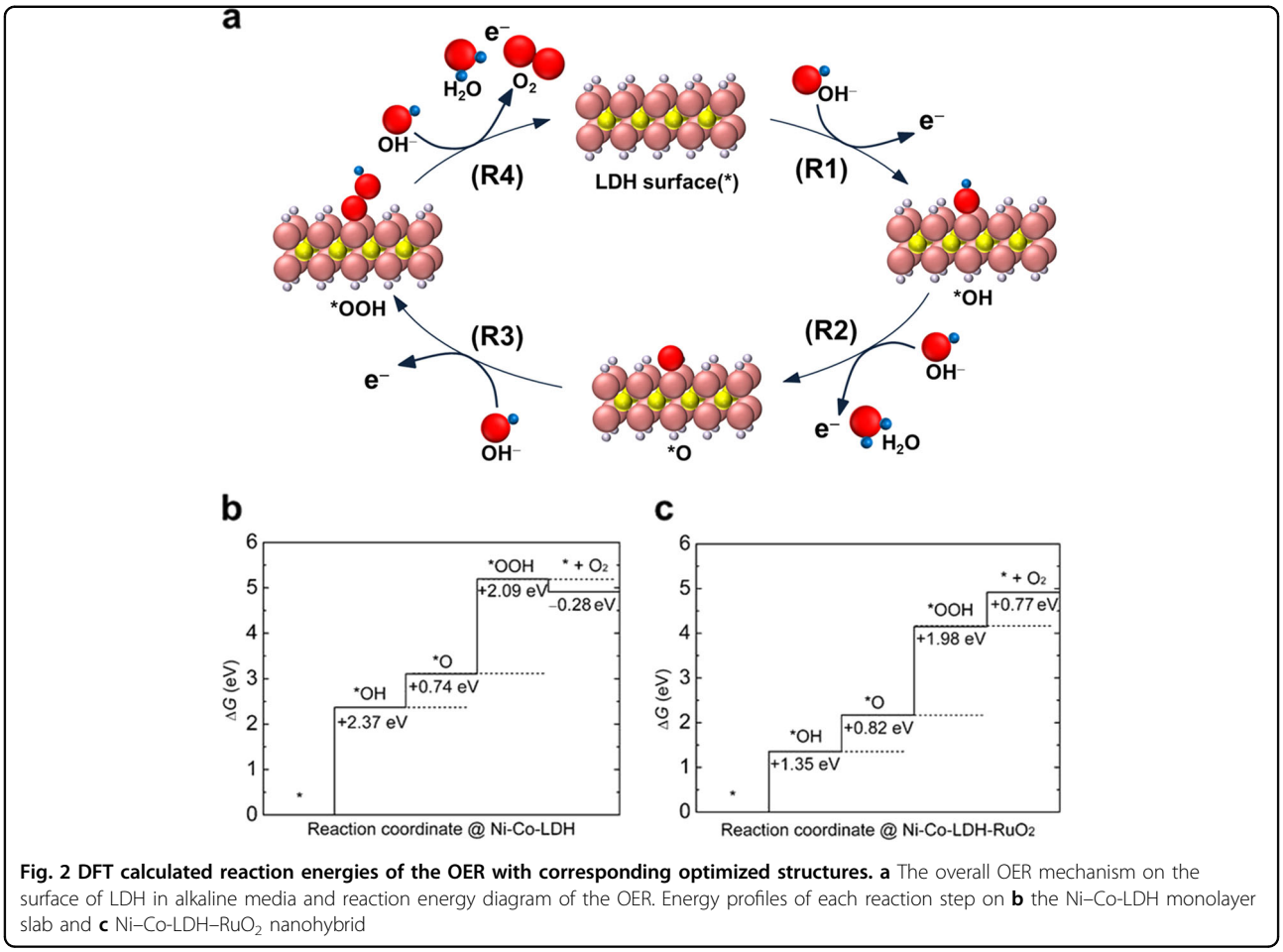

Fig. 2 DFT calculated reaction energies of the OER with corresponding optimized structures. a The overall OER mechanism on the surface of LDH in alkaline media and reaction energy diagram of the OER. Energy profiles of each reaction step on **b** the Ni–Co-LDH monolayer slab and **c** Ni–Co-LDH–RuO_2 nanohybrid

Results and discussion

DFT calculations

The effect of hybridization with RuO_2 NSs on the operation mechanism of the OER catalytic activity of Ni–Co-LDH was theoretically investigated by DFT calculations. According to a previous study on the OER pathway in alkaline media[37,38], the OER pathway is described as the adsorption of successive intermediate species on the catalyst (*) as follows (see also Fig. 2a);

$$* + OH^- \rightarrow *OH + e^- \quad (R1)$$
$$*OH + OH^- \rightarrow *O + H_2O + e^- \quad (R2)$$
$$*O + OH^- \rightarrow *OOH + e^- \quad (R3)$$
$$*OOH + OH^- \rightarrow * + O_2 + H_2O + e^- \quad (R4)$$

We consider the catalytically active site as the deprotonated oxygen atom on the LDH surface[37]. As shown in Fig. 2b, the first step of the OER pathway on the Ni–Co-LDH monolayer, i.e., (R1), is calculated to be the most energetically unfavorable step, providing a threshold energy of 2.37 eV. Hybridization with RuO_2 makes the third step (R3) the most energetically unfavorable step with a threshold energy of 1.98 eV (Fig. 2c). As expected from the previous study[17], this result indicates an increase in the binding energy of OH^- species on the LDH layer upon hybridization with RuO_2 NSs. Indeed, the distance between the oxygen atoms of the OH^- species and the Ni–Co-LDH surface decreases from 1.499 to 1.476 Å after the hybridization of LDH with the RuO_2 slab, as shown in Figures S1a and S1b in the Supplementary Information. The origin of the enhanced binding energy of OH^- species on the nanohybrids can be found in the electronic interaction between the LDH and RuO_2 layers. From the DFT-optimized structures, we find that the interlayer distance between RuO_2 and LDH is close enough to allow direct orbital-orbital interaction; the top-most oxygen atoms of RuO_2 NSs and bottom-most hydrogen atoms of Ni–Co-LDH NSs are separated by only 1.86 Å.

As shown in the density of state analysis of Fig. 3, the occupied Ni 3*d* states in the middle of the bandgap of Ni–Co-LDH (Fig. 3a) are located close to the lowest unoccupied states of the RuO_2 slab (Fig. 3b). Thus, after hybridization, significant mixing of the electronic structures of RuO_2 and LDH occurs (Fig. 3c), resulting in charge transfer from LDH to RuO_2 (Fig. 3d) and a formation of states at the Fermi level elevating the electrical conductivity of the catalyst. To quantify the amount of

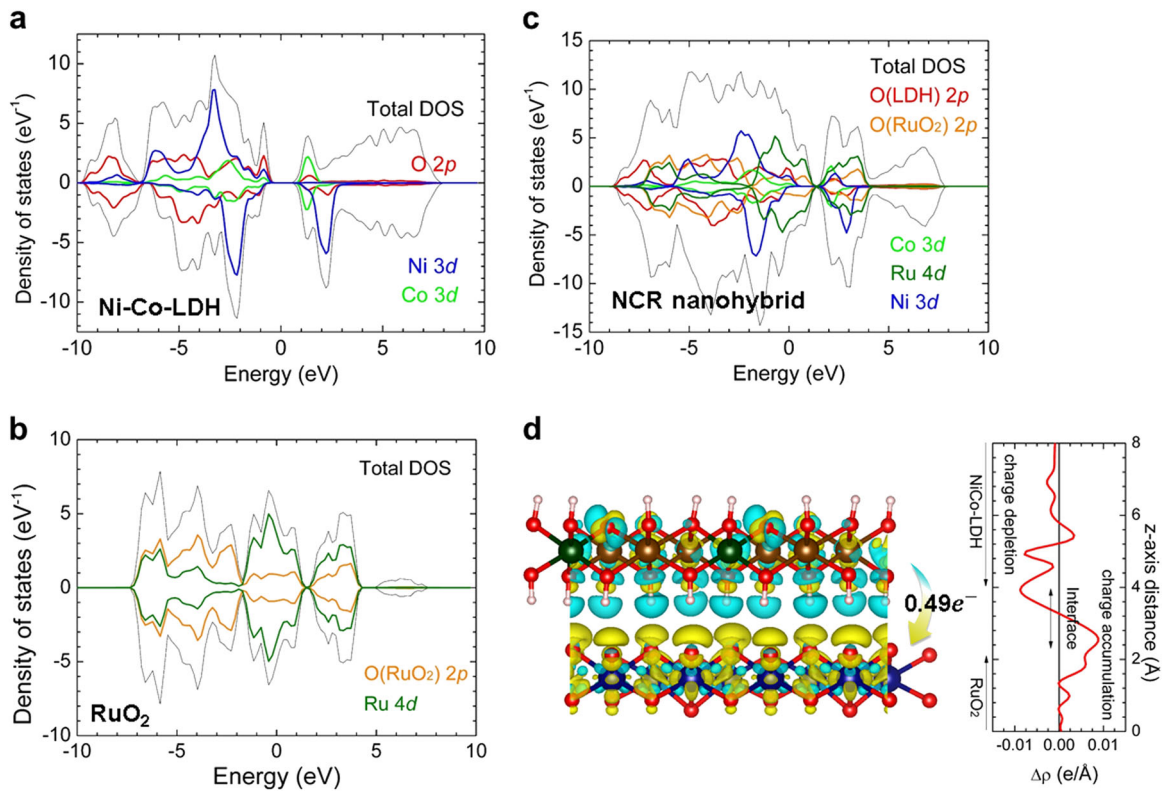

Fig. 3 The density of states (DOS) and charge difference map of the NCR nanohybrid model. The DOS of the **a** Ni–Co-LDH slab model, **b** RuO_2 NS model, and **c NCR** nanohybrid model, where the Fermi level is set to zero. **d** The three-dimensional charge difference map at the isosurface level of $1.00\Delta\rho_{max}$ (100% of the maximum value of $\Delta\rho$), where charge accumulation and depletion are shown in yellow and cyan, respectively, and the corresponding planar averaged charge difference along the surface normal direction is shown on the right. Atoms in the structure are colored by white for H, red for O, brown for Ni, green for Co, and navy for Ru

charge transfer upon hybridization, we further performed a Bader charge analysis for the **NCR** nanohybrid, showing that $0.49e^-$ is transferred to the RuO_2 NSs from Ni–Co-LDH. It was also found that the deprotonated oxygen atom (which serves as the catalytically active center of Ni–Co-LDH) loses the most charge ($0.08e^-$) among the oxygen atoms of Ni–Co-LDH. Thus, the present DFT calculation confirmed our speculation that charge transfer from Ni–Co-LDH to RuO_2 NSs makes the oxygen atom of LDH more electrophilic, and thus, hybridization with RuO_2 NSs enhances the adsorption of OH^- on the Ni–Co-LDH, leading to a decrease in the overpotential for OER.

Structural and morphological characterizations of the NCR nanohybrids

Based on the results of the DFT calculations, the exfoliated Ni–Co-LDH NSs were hybridized with a small amount of RuO_2 NSs to experimentally verify the usefulness of RuO_2 NS hybridization in improving the OER efficiency of a LDH material. As plotted in Fig. 4a, all the present **NCR** nanohybrids as well as the pristine Ni–Co-LDH show XRD peaks typical of the Ni–Co-LDH phase, indicating stabilization of the LDH in the present nanohybrids. In contrast to the Bragg reflections of the LDH phase, the XRD peaks of layered RuO_2 are not discernible, reflecting the homogeneous dispersion of RuO_2 NSs and/or its low concentration below the detection limit. However, the incorporation of RuO_2 NSs into the present **NCR** nanohybrids is obviously evidenced by the Ru K-edge extended X-ray absorption fine structure and EDS-line scanning analyses, which show the presence of RuO_2 NSs in these materials (see Figures S4 and S5 in the Supplementary Information). As shown in the FE-SEM images of Fig. 4b, the exfoliation of Ni–Co-LDH into monolayered NSs induces a marked decrease in the lateral dimension of the LDH crystallites due to severe elastic deformation caused by the expansion of the interlayer spacing during the exfoliation process (see Figure S6 in the Supplementary Information). The **NCR** nanohybrids show house-of-cards-type stacking structures, reflecting the creation of mesopores upon hybridization. The HR-TEM image clearly demonstrates the intimate stacking of the oppositely charged Ni–Co-LDH and RuO_2 NSs.

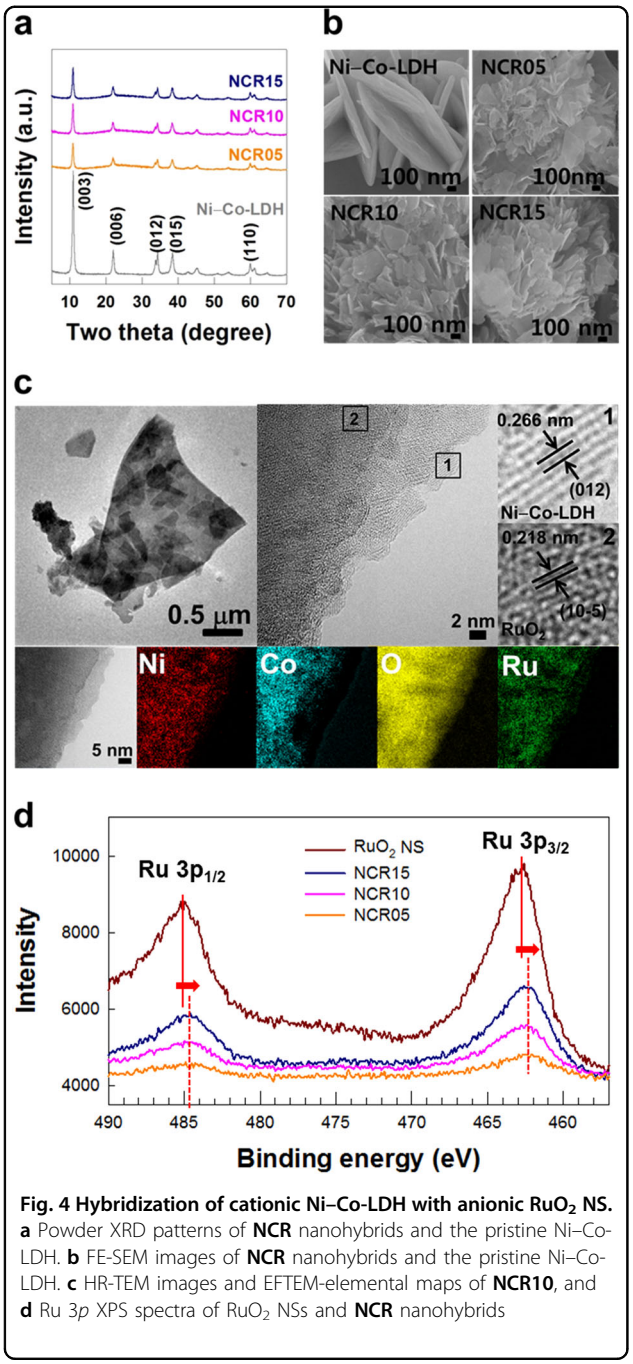

Fig. 4 Hybridization of cationic Ni–Co-LDH with anionic RuO_2 NS. **a** Powder XRD patterns of **NCR** nanohybrids and the pristine Ni–Co-LDH. **b** FE-SEM images of **NCR** nanohybrids and the pristine Ni–Co-LDH. **c** HR-TEM images and EFTEM-elemental maps of **NCR10**, and **d** Ru 3*p* XPS spectra of RuO_2 NSs and **NCR** nanohybrids

As seen clearly from Figure S7 in the Supplementary Information, the exfoliated RuO_2 NSs have a large lateral dimension of several micrometers, which is much greater than that of the Ni–Co-LDH NSs (~100–200 nm). As illustrated in Fig. 4c, clear lattice fringes corresponding to the (0, 1, 2) plane of Ni–Co-LDH and the (1, 0, −5) plane of RuO_2 are obviously observed in the present HR-TEM image, confirming the intimate hybridization between the two kinds of NSs. Moreover, the EFTEM-elemental mapping analysis provides further evidence for nanoscale mixing between the LDH and RuO_2 NSs, showing the uniform distribution of Ru, Ni, Co, and O in all parts of **NCR10**. The molar ratios of LDH:RuO_2 were determined to be 1:0.007, 1:0.013, and 1:0.021 for **NCR05**, **NCR10**, and **NCR15**, respectively.

The stabilization of Ni–Co-LDH in the **NCR** nanohybrid was further evidenced by the observation of the typical IR band of this LDH phase (Figure S8 in the Supplementary Information). Of prime importance is that the weak but distinct IR band of the RuO_2 phase appears at 470 cm^{-1} for both **NCR10** and the RuO_2 NSs, confirming the incorporation of RuO_2 NSs into the present nanohybrid. The coexistence of Ni–Co-LDH and RuO_2 NSs in the present **NCR** nanohybrids was also confirmed by the Ni K-, Co K-, and Ru K-edge X-ray absorption near-edge structure (XANES) spectroscopic analyses (see Figure S9 in the Supplementary Information). In the Ru K-edge XANES spectra, all the **NCR** nanohybrids exhibit spectral features similar to those of the layered $Na_{0.2}RuO_2$, indicating the maintenance of the original layered lattice structure of the RuO_2 NSs upon hybridization with LDH. Similarly, in the Ni K- and Co K-edge XANES region, the overall spectral features of the **NCR** nanohybrids are nearly identical to those of the pristine Ni–Co-LDH, underscoring the incorporation of the Ni–Co-LDH lattice in the present nanohybrids. The N_2 adsorption-desorption isotherm measurements demonstrate that all the present **NCR** nanohybrids possess slightly larger Brunauer-Emmett-Teller surface areas (~35 $m^2 g^{-1}$) than that of the pristine Ni–Co-LDH (~30 $m^2 g^{-1}$), Figure S10 in the Supplementary Information. Despite the very small amount of RuO_2 NSs incorporated, hybridization with RuO_2 NSs leads to a slight but distinct increase in the surface area, indicating the usefulness of RuO_2 addition in enhancing the porosity of LDH materials.

The interfacial charge transfer between the hybridized components was experimentally verified with a surface-sensitive XPS technique. As plotted in Fig. 4d, two Ru $3p_{3/2}$ and $3p_{1/2}$ XPS peaks show lower binding energies of 462.4 and 484.8 eV for **NCR05**, 462.5 and 484.8 eV for **NCR10**, and 462.4 and 484.7 eV for **NCR15** compared with those for the RuO_2 NSs (462.7 and 485.1 eV), highlighting the Ru oxidation state is lowered upon hybridization with Ni–Co-LDH NS. Conversely, the Ni 2*p* and Co 2*p* XPS peaks display a slight blueshift upon hybridization, confirming an electron transfer from Ni–Co-LDH to RuO_2 NSs, Figure S11 in the Supplementary Information. To further confirm the minute spectral changes upon hybridization with a small amount of RuO_2 NSs (1 wt%), the reference nanohybrid of Ni–Co-LDH with a much larger amount of RuO_2 NSs (10 wt%) was prepared and studied via Ni 2*p* and Co 2*p* XPS measurements. As shown in Figure S11 in the Supplementary Information,

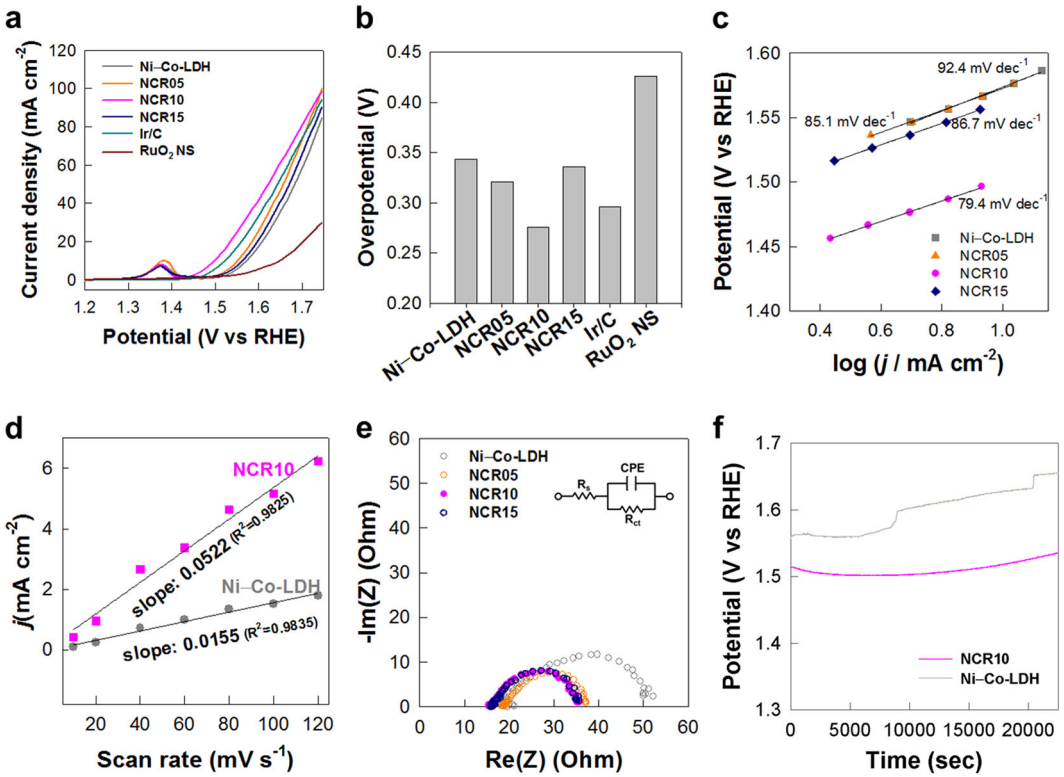

Fig. 5 Electrocatalytic properties of the NCR nanohybrids. a LSV curves. **b** Overpotential required to reach $j = 10$ mA cm^{-2}. **c** Tafel plots of **NCR** nanohybrids and Ni–Co-LDH. **d** Charging current density differences plotted against scan rates of **NCR10** and Ni–Co-LDH. **e** EIS spectra of **NCR** nanohybrids, and **f** chronopotentiometry measurements at $j = 10$ mA cm^{-2} of **NCR10** and Ni–Co-LDH

this reference material displays a much more prominent blueshift in the Ni 2*p* and Co 2*p* XPS peaks, confirming the increase in the oxidation states of Ni and Co upon hybridization with RuO_2 NSs. The present XPS results are in good agreement with the DFT calculation results, showing interfacial electron transfer from Ni–Co-LDH to RuO_2 NSs (Fig. 3d).

Electrochemical performance of the NCR nanohybrids

The influence of the hybridization with RuO_2 NSs on the electrocatalytic activity of Ni–Co-LDH was examined for the OER process ($4OH^- \rightarrow 2H_2O + 4e^- + O_2\uparrow$). As plotted in Fig. 5a, all the present materials show a small peak between 1.3 and 1.4 V in the LSV curves, which corresponds to the oxidation of Ni^{2+} and Co^{3+} ions, confirming the main role of Ni–Co-LDH in the electrochemical activities of these materials[39]. The **NCR** nanohybrids display much smaller on-set potentials with a greater current density than that of the pristine Ni–Co-LDH, highlighting the beneficial effect of hybridization with RuO_2 NSs. Figure 5b presents the overpotentials of the present materials at a current density (*j*) of 10 mA cm^{-2}, which were taken from the LSV curves in Fig. 5a. The overpotential of Ni–Co-LDH is lowered by the incorporation of RuO_2 NSs. Among the present nanohybrids, **NCR10** shows the best electrocatalytic performance with an overpotential of 276 mV at 10 mA cm^{-2}, which is 67 mV lower than that of Ni–Co-LDH, as predicted by the DFT calculations. Of prime importance is that the OER electrocatalyst performance of this material is the best with the smallest overpotential among all reported data on Ni–Co-LDH-based materials (see Table S1 in the Supplementary Information). Although RuO_2 is one of the best electrocatalysts for OER[40–42], the present **NCR** nanohybrid displays a better electrocatalytic performance for OER than the RuO_2 NSs. In comparison with rutile-type RuO_2 nanoparticles[42], the layered RuO_2 NSs show a lower OER activity. Generally, there are many factors affecting the OER activity of inorganic solids, such as the crystal structure, electronic structure, particle size, and degree of hydration[43,44]. An excellent OER electrocatalytic activity has been reported only for rutile RuO_2 nanoparticles and not for layered RuO_2 NSs[45]. Thus, the inferior OER activity of RuO_2 NSs is attributable to its unique layered structure. Considering the inferior OER activity of layered RuO_2 NSs, the observed excellent OER electrocatalytic performance of **NCR** is interpreted to be a result of the synergistic coupling effect of two kinds of

NSs. The beneficial effect of nanoscale hybridization with RuO_2 NSs on the electrocatalytic activity of LDH is further evidenced by the OER electrocatalytic performance of **NCR** that is superior to that of a physical mixture of Ni–Co-LDH NSs and RuO_2 NSs. As shown in Figure S12 in the Supplementary Information, the electrocatalytic performance of the obtained physical mixture is markedly poorer than that of the **NCR** nanohybrid, underscoring the importance of nanoscale mixing between Ni–Co-LDH and RuO_2.

The OER catalytic kinetics of the present nanohybrids was also examined by calculating the Tafel slope. As shown in Fig. 5c, all the **NCR05**, **NCR10**, and **NCR15** nanohybrids exhibit smaller Tafel values, i.e., 85.1, 79.4, and 86.7 mV dec^{-1}, respectively, than the pristine Ni–Co-LDH (92.4 mV dec^{-1}) and the physical mixture of Ni–Co-LDH NSs and RuO_2 NSs (93.0 mV dec^{-1}), highlighting the significant improvement in the OER kinetics upon nanoscale hybridization with RuO_2 NSs. The smallest Tafel value occurs for **NCR10**, which is in good agreement with the high OER activity of this material. The electrochemically active surface area (ECSA) was also estimated from the plot of the charging current versus scan rate measured by CV, and the slope of this plot is equivalent to twice that of the ECSA. As presented in Fig. 5d, the ECSA of **NCR10** is 162% greater than that of Ni–Co-LDH, strongly suggesting effective exposure of the edge sites of NSs upon the exfoliation-restacking process. Figure 5e shows the Nyquist plots of the **NCR** nanohybrids and the pristine Ni–Co-LDH at an applied potential of 1.6 V (vs. RHE) with the simulated fits. As shown in the EIS data in Fig. 5e, the semicircle reflecting charge transfer resistance (R_{ct}) decreases upon hybridization with RuO_2 NSs. According to the fitting analysis using the equivalent circuit, the nanohybrids of **NCR05**, **NCR10**, and **NCR15** have R_{ct} values of 20.6, 19.0, and 19.3 Ω, respectively, which are smaller than that of the pristine Ni–Co-LDH (34.38 Ω), indicating improvement in the charge transfer kinetics at the interfacial region upon hybridization with RuO_2 NSs. Among the present materials, **NCR10** shows the smallest semicircle with the fastest electron transfer rate and smallest R_{ct}. Since the R_{ct} value corresponds to the electrochemical impedance for ion migration into the interfacial region near electrochemically active sites of electrocatalysts during the OER process, this parameter is dependent on both the diffusion rate of the reactant ions into the interfacial region and the electrical conductivity of the electrocatalyst. The content of electrocatalytically active LDH NSs has a significant influence on the R_{ct} because promotion of the OER process will increase the ion diffusion rate into the interfacial region of the electrochemically active sites by enhancing the consumption of reactant ions. Additionally, the content of highly conductive RuO_2 NSs also affects the R_{ct} value by increasing the electrical conductivity of the **NCR** electrocatalyst. Thus, there must be an optimal ratio of LDH/RuO_2 to minimize the charge transfer resistance of **NCR**. The present EIS results indicate that the **NCR10** nanohybrid possesses an optimal ratio of RuO_2/LDH to minimize the R_{ct}.

As plotted in the chronopotentiometry data in Fig. 5f, Ni–Co-LDH exhibits a marked increase in potential after ~8000 s, whereas the potential of **NCR10** retains its initial value up to ~16,500 s, highlighting the remarkable improvement in the electrochemical stability upon hybridization with conductive RuO_2 NSs. Over a longer period, the **NCR10** material still shows good long-term stability superior to that of the pristine Ni–Co-LDH, Figure S13 in the Supplementary Information. Since the LDH has poor electrical conductivity, the accumulation of charge upon the application of an electrical potential leads to redox-induced degradation of the LDH lattice and less electrochemical stability. Hybridization with highly conductive RuO_2 NSs increases the electrical conductivity of the hybridized material, resulting in a decrease in the charging effect and an improvement in the electrochemical stability upon hybridization[35]. In addition, the decreased aggregation of LDH crystals and formation of a porous stacking structure upon hybridization with RuO_2 NSs can also contribute to the enhanced electrochemical stability of the **NCR** nanohybrids[46,47]. Of prime importance is that **NCR10** displays a higher stability than rutile RuO_2 and commercial Ir/C electrocatalysts, as shown in Figure S14 in the Supplementary Information. The present findings clearly demonstrate the high efficiency of RuO_2 NSs as an additive to optimize the electrocatalytic performance of LDH materials.

Hybridization of cationic Ni–Fe-LDH NSs with anionic RuO_2 NSs

To verify the universal validity of hybridization with RuO_2 NSs, exfoliated Ni–Fe-LDH NSs were also hybridized with RuO_2 NSs to synthesize the **NFR10** nanohybrid. Similar to the **NCR** nanohybrids, the **NFR10** nanohybrid shows typical Bragg reflections of the Ni–Fe-LDH phase without any impurity peaks, indicating the presence of Ni–Fe-LDH in this material (see Figure S15 in the Supplementary Information). The formation of the homogeneously hybridized **NFR10** material was confirmed by a TEM analysis (Fig. 6a), showing the anchoring of smaller LDH NSs with (0, 1, 5) lattice fringes on the surfaces of larger RuO_2 NSs with (1, 0, −2) lattice fringes. The uniform hybridization between the RuO_2 NSs and Ni–Fe-LDH NSs was further evidenced by the EFTEM-elemental mapping results, which showed the Ru, Ni, Fe, and O elements are homogeneously distributed in all parts of **NFR10**. As shown in the LSV curves in Fig. 6b,

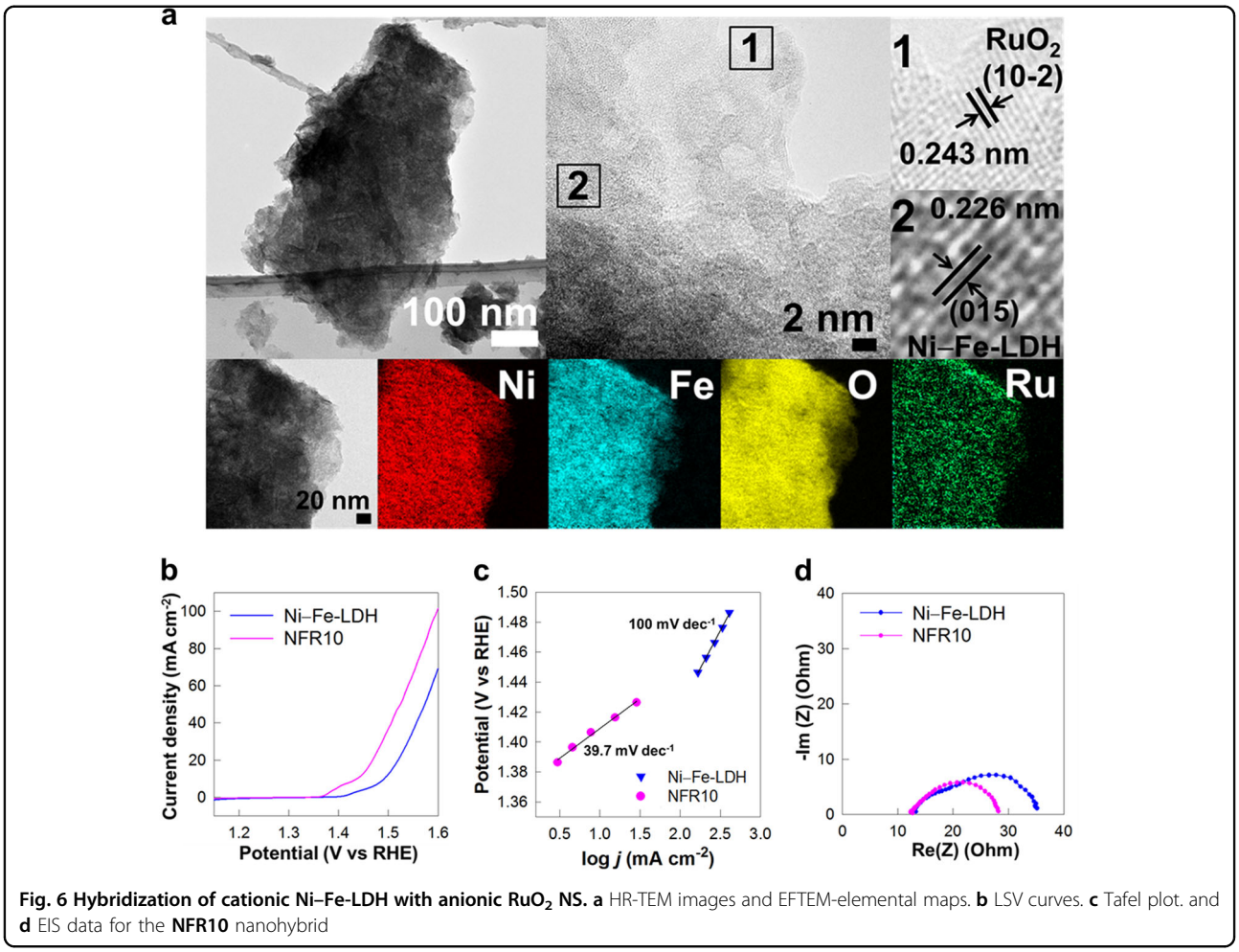

Fig. 6 Hybridization of cationic Ni–Fe-LDH with anionic RuO_2 NS. a HR-TEM images and EFTEM-elemental maps. **b** LSV curves. **c** Tafel plot. and **d** EIS data for the **NFR10** nanohybrid

NFR10 is much more electrocatalytically active for OER than the precursor Ni–Fe-LDH; **NFR10** shows a very small overpotential of 207 mV at 10 mA cm^{-2}, which is much lower than that of pristine Ni–Fe-LDH (261 mV). As plotted in Fig. 6c, **NFR10** has a much smaller Tafel value of 39.7 mV dec^{-1} than that of Ni–Fe-LDH (100 mV dec^{-1}), indicating an improvement in the OER kinetics upon hybridization with RuO_2 NSs. This result highlights the beneficial effect of hybridization with RuO_2 NSs on the OER activity of Ni–Fe-LDH. Table S1 in the Supplementary Information shows that the observed overpotential of **NFR10** is one of the lowest values among those reported in previous studies on Ni–Fe-LDH-based electrocatalysts. According to the EIS analysis (Fig. 6d), the diameter of the semicircle reflecting the charge transfer resistance is smaller for **NFR10** than pristine Ni–Fe-LDH, confirming the promotion of charge transfer kinetics upon hybridization with RuO_2 NSs. The present experimental findings provide strong evidence for the universal merit of RuO_2 NSs as an additive for exploring novel, efficient OER electrocatalysts in terms of strong electronic coupling with inorganic electrocatalysts and the resulting improvement in RDS kinetics.

Discussion

The combination theoretical and experimental study presented here clearly demonstrates that kinetic control of the RDS of an electrocatalytic reaction can provide a rational method to explore high-performance OER electrocatalysts with a remarkable decrease in overpotentials. The DFT calculations highlight the efficient role of RuO_2 NSs as an electron acceptor in increasing the electrophilicity of hybridized inorganic layers and enhancing the surface adhesion of OH^- and/or $OOH^\bullet$ species on the surface of LDH. This leads to a remarkable decrease in the activation energy of the RDS upon hybridization with RuO_2 NSs. Based on this theoretical calculation, highly efficient OER activities with remarkably lower overpotentials and excellent electrochemical stabilities can be achieved by intimate hybridization between electrocatalytically active LDH NSs and electron-withdrawing RuO_2 NSs. Nanoscale hybridization between exfoliated

LDH and RuO_2 NSs can be easily achieved by an electrostatically derived self-assembly process because of their opposite surface charges. The resulting **NCR10** and **NFR10** boast excellent OER performances with very small overpotentials of 276 and 207 mV at 10 mA cm^{-2}, respectively, as well as improved charge transfer kinetics and electrochemical stability. It is worthwhile to note here that the DFT calculation predicts a much greater change in the threshold energies of Ni–Co-LDH upon RuO_2 hybridization (2.37 eV → 2.26 eV; 110 meV decrease) compared with the shift of the on-set potential from 1.572 V for Ni–Co-LDH NS to 1.505 V for the **NCR** nanohybrid (68 mV decrease). We determined that the theoretical comparison of a single LDH layer versus an LDH–RuO_2 bilayer (corresponding to the case when every LDH layer develops an interaction with RuO_2) resulted in a more drastic change in the calculated overpotential than the experimental values. Even with the much smaller content of RuO_2 NSs (1 wt%) in **NCR10** compared with that in the theoretical model of a 1:1 LDH–RuO_2 bilayer, **NCR10** displays an OER activity slightly inferior but somewhat comparable to the theoretically predicted activity, highlighting the high efficiency of RuO_2 hybridization in increasing the electrocatalytic activity of the LDH. The present electrochemical results clearly demonstrate the effectiveness of hybridization with electron-withdrawing inorganic NSs in remarkably improving the electrocatalytic functionality of polar, inorganic solids. Controlling the RDS via hybridization with a small amount of electron-withdrawing RuO_2 NSs provides a novel, rational method to explore economically feasible efficient electrocatalysts. In comparison with previously reported, efficient, RuO_2-based OER electrocatalysts showing low overpotentials of 360 mV for commercial 20 wt% RuO_2/C (Ru: ~14 wt%)[39], 290 mV for RuO_2-loaded on Ti plates (Ru: ~74 wt%)[40], and 220 mV for (100)-oriented rutile RuO_2 (Ru: ~74 wt%)[41], the present **NFR10** nanohybrid with a much smaller Ru content of ~0.7 wt% displays a much lower overpotential of 207 mV at 10 mA cm^{-2}, highlighting the usefulness of the present synthetic strategy in exploring novel, efficient electrocatalysts. The very low Ru content of the present nanohybrid provides this material with a high level of economic feasibility over that of conventional RuO_2-based OER electrocatalysts. It is worthwhile to mention that despite the rarity of Ru, the price of Ru is still 12 times cheaper than that of Ir, which is also utilized as an OER electrocatalyst[48], underscoring the validity of the present nanohybrid as an economically feasible electrocatalyst. Considering the fact that the 2D morphology of inorganic NSs provides effective anchoring sites for diverse inorganic electrocatalysts, the present synthetic strategy with electron-withdrawing or electron-donating inorganic NSs will evoke a great deal of research on the development of new, high-performance, hybrid electrocatalysts. A high flexibility in the compositional control of inorganic NSs via cation- and anion-substitution allows us to optimize the electronic structure and ability to accept or donate electron density of hybridized electrocatalysts[49]. Our current project is exploring novel, economically feasible, efficient electrocatalysts for HER, ORR, and CO_2 reduction reaction via hybridization of nanostructured transition metal hydroxides/oxides with electron-withdrawing/-donating inorganic NSs.

Acknowledgements
This work was supported by the National Research Foundation of Korea (NRF) grant funded by the Korea government (MSIP) (No. NRF-2017R1A2A1A17069463) and by the Korea government (MSIT) (No. NRF-2017R1A5A1015365). The experiments at PAL were supported in part by MOST and POSTECH.

Author details
[1]Center for Hybrid Interfacial Chemical Structure (CICS), Department of Chemistry and Nanoscience, College of Natural Sciences, Ewha Womans University, Seoul 03760, Republic of Korea. [2]Department of Chemistry and Graduate School of EEWS, Korea Advanced Institute of Science and Technology (KAIST), Daejeon 34141, Republic of Korea. [3]National Institute for Nanomaterials Technology (NINT), Pohang University of Science and Technology (POSTECH), Pohang 37673, Republic of Korea

Conflict of interest
The authors declare that they have no conflict of interest.

Supplementary information is available for this paper at https://doi.org/10.1038/s41427-018-0060-3.

Received: 30 October 2017 Revised: 6 March 2018 Accepted: 25 May 2018.
Published online: 23 July 2018

References

1. Su, D. et al. Ruthenium nanocrystal decorated vertical graphene nanosheets@Ni foam as highly efficient cathode catalysts for lithium-oxygen batteries. *NPG Asia Mater.* **8**, e286 (2016).
2. Park, S., Shao, Y., Liu, J. & Wang, Y. Oxygen electrocatalysts for water electrolyzers and reversible fuel cells: status and perspective. *Energy Environ. Sci.* **5**, 9331–9344 (2012).
3. Diaz-Morales, O. et al. Iridium-based double perovskites for efficient water oxidation in acid media. *Nat. Commun.* **7**, 12363 (2016).
4. Su, J. et al. Ruthenium-cobalt nanoalloys encapsulated in nitrogen-doped graphene as active electrocatalysts for producing hydrogen in alkaline media. *Nat. Commun.* **8**, 14969 (2017).
5. Viswanathan, V., Hansen, H. A. & Nørskov, J. K. Selective electrochemical generation of hydrogen peroxide from water oxidation. *J. Phys. Chem. Lett.* **8**, 1157–1160 (2017).
6. Zhong, H.-x. et al. In situ anchoring of Co_9S_8 nanoparticles on N and S co-doped porous carbon nanotube as bifunctional oxygen electrocatalyst. *NPG Asia Mater.* **8**, e308 (2016).
7. Zheng, Y. et al. Molecule-level g-C_3N_4 coordinated transition metals as a new class of electrocatalysts for oxygen electrode reaction. *J. Am. Chem. Soc.* **139**, 3336–3339 (2017).
8. Song, F. & Hu, X. Exfoliation of layered double hydroxides for enhanced oxygen evolution catalysis. *Nat. Commun.* **5**, 4477 (2014).

9. Friebel, D. et al. Identification of highly active Fe sites in (Ni,Fe)OOH for electrocatalytic water splitting. *J. Am. Chem. Soc.* **137**, 1305–1313 (2015).
10. Lu, Z. et al. Ternary NiFeMn layered double hydroxides as highly-efficient oxygen catalysts. *Chem. Commun.* **52**, 908–911 (2016).
11. Hunter, B. M., Hieringer, W., Winkler, J. R., Gray, H. B. & Muller, A. M. Effect of interlayer anions on [NiFe]-LDH nanosheet water oxidation activity. *Energy Environ. Sci.* **9**, 1734–1743 (2016).
12. Jin, X., Lim, J., Lee, N.-S. & Hwang, S.-J. A powerful role of exfoliated metal oxide 2D nanosheet as additives for improving electrocatalyst functionality of graphene. *Electro. Acta* **235**, 720–729 (2017).
13. Tang, C., Wang, H. F., Zhu, X. L., Li, B. Q. & Zhang, Q. Advances in hybrid electrocatalysts for oxygen evolution reactions: rational integration of NiFe layered double hydroxides and nanocarbon. *Part. Part. Syst. Charact.* **33**, 473–486 (2016).
14. Wu, J. et al. A highly active oxygen evolution electrocatalyst: ultrathin CoNi double hydroxide/CoO nanosheets synthesized via interface-directed assembly. *Nano Res.* **9**, 713–725 (2016).
15. Rossmeisl, J., Logadottir, A. & Nørskov, J. K. Electrolysis of water on (oxidized) metal surfaces. *Chem. Phys.* **319**, 178–184 (2015).
16. Rossmeisl, J., Qu, Z.-W., Zhu, H., Kroses, G.-J. & Nørskov, J. K. Electrolysis of water on oxides surfaces. *J. Electroanal. Chem.* **607**, 83–89 (2007).
17. Lee, J. M. et al. A conductive hybridization matrix of RuO_2 two-dimensional nanosheets: a hybrid-type photocatalyst, *Angew. Chem. Int'l. Ed.* **55**, 8546–8550 (2016).
18. Lee, S. et al. Superior additive of exfoliated RuO_2 nanosheet for optimizing the electrode performance of metal oxide over graphene. *J. Phys. Chem. C.* **120**, 11786–11796 (2016).
19. Kresse, G. & Furthmüller, J. Efficiency of ab-initio total energy calculations for metals and semiconductors using a plane-wave basis set. *Comput. Mat. Sci.* **6**, 15–50 (1996).
20. Kresse, G. & Furthmüller, J. Efficient iterative schemes for *ab initio* total-energy calculations using a plane-wave basis set. *Phys. Rev. B* **54**, 11169–11186 (1996).
21. Blöchl, P. E. Projector augmented-wave method. *Phys. Rev. B* **50**, 17953–17979 (1994).
22. Kresse, G. & Joubert, D. From ultrasoft pseudopotentials to the projector augmented-wave method. *Phys. Rev. B* **59**, 1758–1775 (1999).
23. Perdew, J. P., Burke, K. & Ernzerhof, M. Generalized gradient approximation made simple. *Phys. Rev. Lett.* **77**, 3865–3868 (1996).
24. Dudarev, S. L., Botton, G. A., Savrasov, S. Y., Humphreys, C. J. & Sutton, A. P. Electron-energy-loss spectra and the structural stability of nickel oxide: an LSDA+U study. *Phys. Rev. B* **57**, 1505–1509 (1998).
25. Qian, L. et al. Trinary layered double hydroxides as high-performance bifunctional materials for oxygen electrocatalysis. *Adv. Energy Mater.* **5**, 1500245 (2015).
26. Sanville, E., Kenny, S. D., Smith, R. & Henkelman, G. An improved grid-based algorithm for Bader charge allocation. *J. Comp. Chem.* **28**, 899–908 (2007).
27. Henkelman, G., Arnaldsson, A. & Jönsson, H. A fast and robust algorithm for Bader decomposition of charge density. *Comput. Mater. Sci.* **36**, 254–360 (2006).
28. Yu, M. & Trinkle, D. R. Accurate and efficient algorithm for Bader charge integration. *J. Chem. Phys.* **134**, 064111 (2011).
29. Momma, K. & Izumi, F. VESTA 3 for three-dimensional visualization of crystal, volumetric and morphology data. *J. Appl. Crystallogr.* **44**, 1272–1276 (2011).
30. Wang, V., Xiao, W., Ma, D.-M., Liu, R.-J. & Yang, C.-M. Structural, electronic, and optical properties of $GaInO_3$: A hybrid density functional study, *J. Appl. Phys.* **115**, 043708 (2014).
31. Linstrom, P. J. & Mallard, W. G. (eds.) NIST Chemistry WebBook, NIST standard reference Database number 69, National Institute of Standards and Technology, Gaithersburg MD, 20899, (retrieved April 27, 2017).
32. Bard, A. J. & Faulkner, L. R. *Electrochemical Methods*. 2nd edn (John Wiley & Sons, Inc: New York, 2001).
33. Kurth, S., Perdew, J. P. & Blaha, P. Molecular and solid-state tests of density functional approximations: LSD, GGAs, and meta-GGAs. *Int. J. Quantum Chem.* **75**, 889–909 (1999).
34. Fukuda, K. et al. Synthesis of nanosheet crystallites of ruthenate with an α-$NaFeO_2$-related structure and its electrochemical supercapacitor property. *Inorg. Chem.* **49**, 4391–4393 (2010).
35. Jiang, J., Zhang, A., Li, L. & Ai, L. Nickel-cobalt layered double hydroxide nanosheet as high performance electrocatalyst for oxygen evolution reaction. *J. Power Sources* **278**, 445–451 (2015).
36. Coronado, E. et al. Spontaneous magnetization in Ni-Al and Ni-Fe layered double hydroxides. *Inorg. Chem.* **47**, 9103–9110 (2008).
37. Dong, Y. et al. A first-principles study of oxygen formation over NiFe-layered double hydroxides surface. *Catal. Lett.* **145**, 1541–1561 (2015).
38. García-Mota, M. et al. Importance of correlation in determining electrocatalytic oxygen evolution activity on cobalt oxides. *J. Phys. Chem. C.* **16**, 21077–21082 (2010).
39. Li, Y., Hasin, P. & Wu, Y. $Ni_xCo_{3-x}O_4$ nanowire arrays for electrocatalytic oxygen evolution. *Adv. Mater.* **22**, 1926–1929 (2010).
40. Jiang, Z.-J. & Jiang, Z. Interaction induced high catalytic activities of CoO nanoparticles grown on nitrogen-doped hollow graphene microspheres for oxygen reduction and evolution reactions. *Sci. Rep.* **6**, 27081 (2016).
41. Pu, Z., Luo, Y., Asiri, A. M. & Sun, X. Efficient electrochemical water splitting catalyzed by electrodeposited nickel diselenide nanoparticles based film. *ACS Appl. Mater. Inerfaces* 8, (4718–4723 (2016).
42. Stoerzinger, K. A., Qiao, L., Biegalski, M. D. & Shao-Horn, Y. Orientation dependent oxygen evolution activities of rutile IrO_2 and RuO_2. *J. Phys. Chem. Lett.* **5**, 1636–1641 (2014).
43. Man, I. C. et al. Universality in oxygen evolution electrocatalysis on oxide surface. *ChemCatChem.* **3**, 1159–1165 (2011).
44. Zhao, Y., Hernandez-Pagan, E. A., Vargas-Barbosa, N. M., Dysart, J. L. & Mallouk, T. E. A high yield synthesis of ligand-free iridium oxide nanoparticles with high electrocatalytic activity. *J. Phys. Chem. Lett.* **2**, 402–406 (2011).
45. Stoerzinger, K. A., Ziao, L., Biegalski, M. D. & Shao-Horn, Y. Orientation-dependent oxygen evolution activities of rutile IrO_2 and RuO_2. *J. Phys. Chem. Lett.* **5**, 1636–1641 (2014).
46. Xia, W.-Y., Li, N., Li, Q.-Y., Ye, K.-H. & Xu, C.-W. Au-$NiCo_2O_4$ supported on three-dimensional hierarchical porous graphene-like material for highly effective oxygen evolution reaction. *Sci. Rep.* **6**, 23398 (2016).
47. Wang, Q. et al. Zinc-air batteries: NiFe layered double hydroxide nanoparticles on Co, N-codoped carbon nanoframes as efficient bifunctional catalysts for rechargeable zinc-air batteries. *Adv. Mater.* **7**, 1700467 (2017).
48. InvestmentMine Home page. http://www.infomine.com/investment/metal-prices/ (accessed Aug 5, 2016).
49. Lee, J. M. et al. A crucial of Rh substituent ion in photoinduced internal electron transfer and enhanced photocatalytic activity of CdS-$Ti_{(5.2-x)}Rh_{x/2}O_2$ nanohybrids. *Small* **11**, 5771–5780 (2015).